INTERFACE

royalsocietypublishing.org/rsif

CC BY

Research

Cite this article: Benerradi R, Dakos V, Cano AV. 2026 Sensitivity of fish stock trajectories to climate forcing and human exploitation at a global scale. *J. R. Soc. Interface* **23**: 20251040.
https://doi.org/10.1098/rsif.2025.1040

Received: 8 October 2025
Accepted: 11 June 2026

Subject Category:
Life Sciences - Mathematics interface

Subject Areas:
ecosystem

Keywords:
fisheries productivity, causal inference, climate impacts, harvest pressure

Author for correspondence:
Alejandro V Cano
e-mail: alejandro.viloria-cano@ird.fr

THE ROYAL SOCIETY
PUBLISHING

Sensitivity of fish stock trajectories to climate forcing and human exploitation at a global scale

Raphaël Benerradi[1,2], Vasilis Dakos[1] and Alejandro V Cano[1,3]

[1]Institut des Sciences de l'Évolution de Montpellier (ISEM), Univ. de Montpellier, CNRS, IRD, Montpellier, France
[2]LIRMM, INRIA, Univ Montpellier, CNRS, Montpellier, France
[3]MARBEC Laboratory, Univ. Montpellier, CNRS, Ifremer, IRD, Sète, France

RB, 0009-0002-9020-0702; VD, 0000-0001-8862-718X; AVC, 0000-0003-4728-8489

Global fisheries are under increasing pressure from overfishing and climate change, threatening marine biodiversity and food security. Disentangling the impacts of these two drivers is essential for sustainable management, yet it remains a major challenge due to the complex nature of marine ecosystems. Here, we utilize a data-driven empirical dynamic modelling framework to assess causal relationships between harvest rate, sea surface temperature (SST), and the productivity of 155 fish stocks worldwide. Our analysis identifies fishing pressure as the most prevalent driver of stock productivity, with a causal link detected in 71 stocks (45.8%). SST was also identified as a significant driver of productivity in 39 stocks (25.2%). While the impact of harvest rate was stock-specific, being either positive or negative, the influence of SST was predominantly negative and, in many cases, intensified over time. These results provide empirical evidence that direct exploitation and climate warming are systematically impacting fish stock productivity, with direct exploitation emerging as the predominant driver across stocks. This predominance suggests that improved harvest management could help buffer or mitigate some of the negative impacts of climate warming on fisheries productivity.

1. Introduction

Fisheries are a vital component of global food security, yet their sustainability is under significant threat. The proportion of marine stocks fished within biologically sustainable levels continues to decline, reaching just 62.3% of sustainably fished stocks in 2021 [1]. Among the various drivers affecting fish stock trajectories, fishing pressure is a major one. Climate change has impacts on marine fish stocks and ecosystem services—especially food provisioning—through warming temperatures affecting stock distribution and productivity, acidification, deoxygenation, shifts in primary productivity or influxes of particulate organic carbon (POC) [2–6]. These drivers are not independent; overfishing can amplify the vulnerability of fish stocks to climate impacts, undermining their resilience and long-term viability [2,3,7]. Classical surplus-production theory predicts a unimodal relationship between stock biomass and surplus production, such that moderate harvest rates can increase surplus production by fishing down from unfished biomass, whereas excessive exploitation erodes biomass and reduces productivity below levels that can sustain maximum sustainable yield [8–11]. In this context, harvest rate is used to guide management, but it can be altered when environmental changes shift the underlying productivity of the stock. Understanding how fishing pressure and climate-driven changes in temperature jointly affect productivity—and whether their effects are

© 2026 The Authors. Published by the Royal Society under the terms of the Creative Commons Attribution License http://creativecommons.org/licenses/by/4.0/, which permits unrestricted use, provided the original author and source are credited.

Downloaded from royalsocietypublishing.org/rsif/article-pdf/doi/10.1098/rsif.2025.1040/6157114/rsif.2025.1040.pdf
by guest
on 15 August 2026

positive or negative at a given point in time—is therefore critical for interpreting stock status, anticipating productivity regime shifts and designing harvest strategies that remain robust under changing environmental conditions. In particular, management decisions depend not only on identifying which drivers are most important but also on understanding the direction and sign of their effects on productivity, so that changes in fishing pressure or warming can be interpreted causally rather than as mere correlations.

Yet, identifying the global drivers of fish stocks and their relative importance remains a challenging and difficult task [12]. The Intergovernmental Science-Policy Platform on Biodiversity and Ecosystem Services (IPBES) Global Assessment provides an estimate of the relative importance of the drivers of global decline in marine ecosystems based on a meta-analysis that identifies direct exploitation as the most important driver, followed by changes in ocean use and climate change [13]. While the attribution methodologies provide outstanding information on the drivers of biodiversity change, they mostly rely on mechanistic models, species distribution models, controlled environment experiments and expert knowledge—e.g. thresholds identified by ecophysiology. These methods allow us to consider a wide range of information through knowledge of the effects involved. However, few studies seem to consider the inference of global causal effects based on data-driven frameworks [14,15].

Here, we employ a data-driven framework and infer causality directly from empirical time series. Specifically, we apply empirical dynamic modelling (EDM) [16–18] to a global database of 155 commercially exploited fish stocks to assess and quantify the causal drivers of stock productivity. We use convergent cross-mapping (CCM) [18], strengthened with a stringent null model testing procedure, to identify causal links between stock productivity and two key drivers: fishing pressure (harvest rate) and sea surface temperature (SST). We then quantify the direction, strength and temporal trend of these detected causal effects. This data-driven, non-parametric (i.e. equation-free) approach allows us to investigate the nonlinear dynamics governing fisheries and provide a robust, large-scale assessment of the sensitivity of marine ecosystems to both human exploitation and environmental forcing.

2. Methods

2.1. Dataset

We used the RAM Legacy Stock Assessment Database version v4.66 (RAMLDB), which consists of fishery-related data for 1594 commercially exploited marine fish and invertebrate stocks [19]. This dataset provides the annual time series of total biomass, total catch and harvest rate. Based on the total biomass and total catch, we computed time series of the stock productivity (SProd) for each year for each stock. Productivity quantifies the biomass produced by a fish stock that exceeds what is needed for its own reproduction and maintenance, hence representing a measure of the ability to sustainably support future harvesting. It is defined as follows: $S(t) = B(t+1) - B(t) + C(t)$, where $S(t)$ is the productivity (denoted SProd) at time t (years), B is the total biomass and C is the total catch [8,20]. We then divided the productivity by the average total biomass of the fish stock along the time series, to normalize the surplus production relatively to the average size of the fish stock.

In the RAMLDB, harvest rate U refers to either the exploitation rate or fishing mortality, depending on the stock. We use the harvest rate U normalized by the harvest rate at the maximum sustainable yield (MSY) biological reference point (U_{MSY}), derived from stock assessment models. This normalized harvest rate is denoted as HRate. Specifically, HRate = U/U_{MSY}. Thus, a fish stock with HRate = 1 is at the management target reference point, a fish stock with HRate > 1 is overfished with respect to the harvest rate and underfished if HRate < 1. SST was extracted from the Met Office HadISST1 dataset [21]. To match the SST to each fish stock, we collected the geographic boundaries of the stocks in the RAMLDB, available at Christopher Free's website: https://chrismfree.com/ram-legacy-stock-boundary-database/. For each fish stock and for each year, we computed the geographic average within the fish stock boundary of the annual average of SST. We only kept fish stocks with more than 40 consecutive years of data for productivity, harvest rate and SST, as previously done in the application of the EDM framework on fish stocks [22,23]. After filtering, we got 155 fish stocks for analysis. An overview of the dataset is presented in figure 1, and time series for all stocks can be found in figures S1–S4 in the supplementary material. We conducted the analysis in R version 4.4.2, mainly using the R package `rEDM` version 1.15.4.

2.2. Embedding dimensions: simplex projection

EDM relies on representing the dynamics of a system—i.e. multiple variables changing through time—by using delay embeddings—some of these variables with their lags changing through time. The Simplex projection allows us to assess the quality of this representation. Let us consider a time series of n variables associated with a given fish stock for each time step t from 1 to T. We denote the state variable at each time step t with the vector $\mathbf{x}_t = \left(x_1(t), \ldots, x_n(t)\right)$. The time series is denoted with the indexed family $\left(\mathbf{x}_t\right)_{t\in\{1,\ldots,T\}}$. For instance, in our case, $n = 3$ and x_1, x_2 and x_3 are SST, HRate and SProd, respectively. According to Takens' theorem [24], for any $j \in \{1, \ldots, n\}$, for a given integer E^*—where $\frac{E^*-1}{2}$ is the unobserved dimension of the manifold M in which the dynamics is observed—the function $\Phi : M \to \mathbb{R}^{E^*}$ verifying for all t, $\Phi(\mathbf{x}_t) = (x_j(t), x_j(t-1), \ldots, x_j(t-E^*+1))$ is an embedding (i.e. continuous and bijective function onto its image) from the manifold of the dynamics to the manifold in the lag space. In practice, E^* is estimated by a given E_{optimal} (defined below) using the Simplex projection algorithm from the EDM framework (see the supplementary material of Sugihara *et al.* [18]).

Downloaded from royalsocietypublishing.org/rsif/article-pdf/doi/10.1098/rsif.2025.1040/6157114/rsif.2025.1040.pdf
by guest
on 15 August 2026

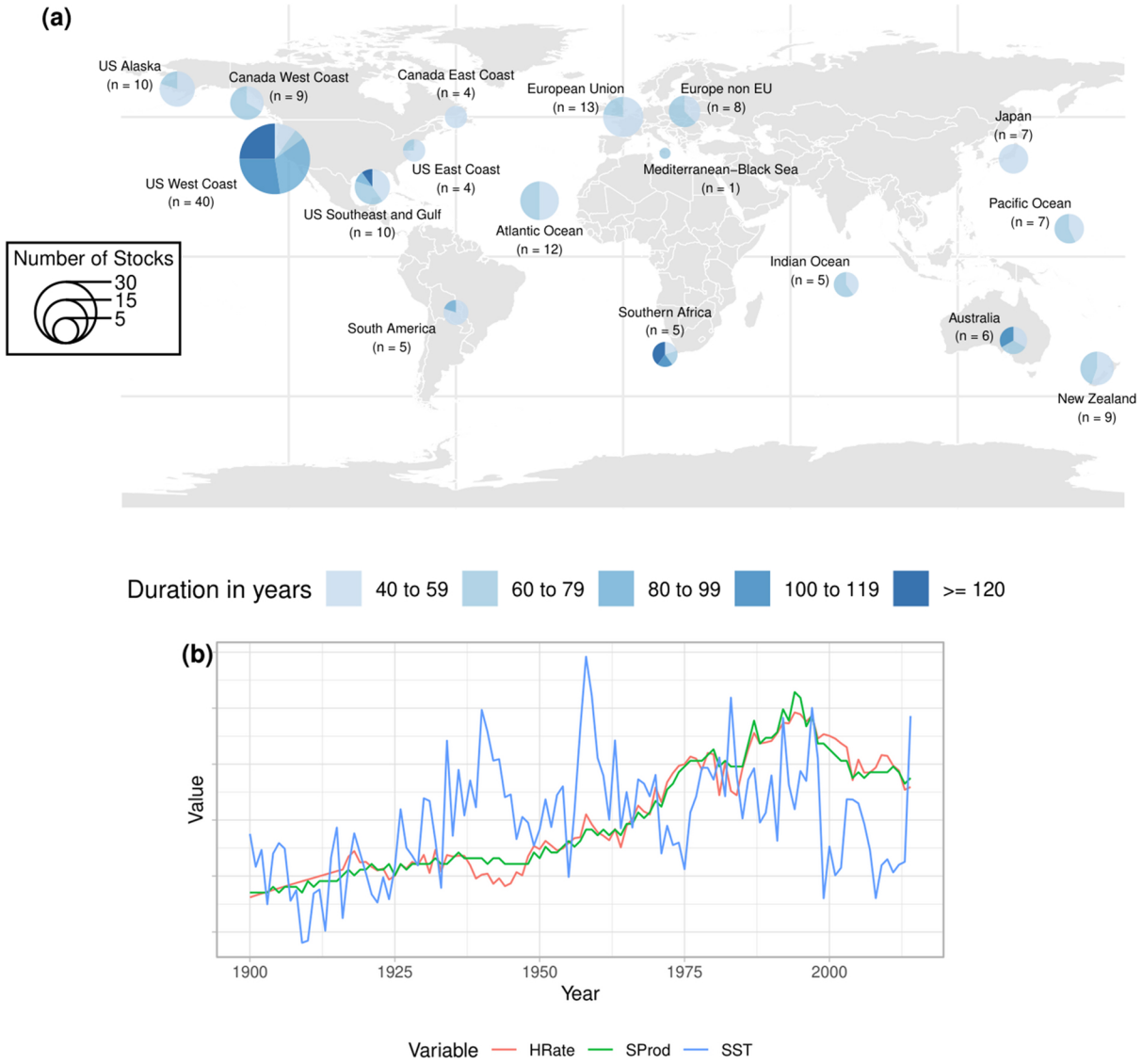


Figure 1. Overview of the processed dataset from the RAM Legacy Database. (a) Pie charts of the duration of the time series located in the region of the fish stock, for the 155 fish stocks analysed in this study. (b) Example of the time series for the fish stock *China rockfish Southern Pacific Coast*; HRate is the harvest rate (U) normalized by the harvest rate at the maximum sustainable yield (U_{MSY}), SST is centred and scaled, and stock SProd is the surplus productivity divided by the mean total biomass along time.

The Simplex projection aims at predicting future values of a variable based on nearest neighbours in a lag space of dimension E. More precisely, for a focal time t^*, $\hat{x}_j(t^*+1)$ is predicted based on the next value of the nearest neighbours of $(x_j(t^*), x_j(t^*-1), \ldots, x_j(t^*-E+1))$, among all other data points in the lag space $\big((x_j(t), x_j(t-1), \ldots, x_j(t-E+1))\big)_{t\neq t^*,\, E\leq t\leq T-1}$. We considered all the other points to be candidates for nearest neighbours, following the implementation of Deyle *et al.* [25], which does not apply an additional temporal exclusion window around the prediction point. This differs from approaches that use an additional filtering depending on the focal time from which the projection is being made [26], which effectively reduces the number of candidates to approximately $T-2(E+1)$. Given the relatively short length of time series considered here, we opted for the Deyle *et al.* [25] scheme to maximize the number of points contributing to the nearest neighbour candidates while still respecting the embedding constraints. Based on the predictions, we get a forecasting skill $\rho(E)$, defined as the correlation between the observed $\big(x_j(t^*+1)\big)_{E\leq t^*\leq T-1}$ and the predicted $\big(\hat{x}_j(t^*+1)\big)_{E\leq t^*\leq T-1}$ over all focal time steps t^*. We tried embedding dimensions E from 2 to 10 to search for the optimal E_{optimal} that was associated with a high forecasting skill $\rho(E_{\text{optimal}})$ [18]. To define E_{optimal}, we consider the trade-off of E_{optimal} being small enough and providing a sufficiently high forecasting skill by selecting the smallest E in the top 20% range of values of forecasting skills. That is, let us note $\rho_{\min}^{(\text{clip})} = \max(0, \min_E(\rho(E)))$ and $\rho_{\max} = \max_E(\rho(E))$. We selected $E_{\text{optimal}} = \min\left\{E;\ \rho(E) \geq \rho_{\min}^{(\text{clip})} + 0.8 \times (\rho_{\max} - \rho_{\min}^{(\text{clip})})\right\}$. The minimum forecasting skill considered is clipped at 0 because a negative forecasting skill means the embedding is not relevant to represent the dynamics in the lag space. If all the forecasting skills $\big(\rho(E)\big)_{E\in\{2,\ldots 10\}}$ are negative, we consider that no embedding dimension allows us to represent the dynamics properly. The Simplex projection was applied using the `EmbedDimension` function from the R package `rEDM`.

Downloaded from royalsocietypublishing.org/rsif/article-pdf/doi/10.1098/rsif.2025.1040/6157114/rsif.2025.1040.pdf
by guest
on 15 August 2026

2.3. Causality assessment: convergent cross mapping

CCM is a method to identify causality between variables in nonlinear dynamical systems that do not verify separability—i.e. the information of a causal variable is not independently unique to this variable [18]. Here, considering the dynamics $\mathbf{x}_{t+1} - \mathbf{x}_t = f(\mathbf{x}_t, t)$, x_i causing x_j refers to the dependence on x_i in the jth coordinate of f [15]. Note that here the definition of causality does not refer to causality found from experimental design.

In the EDM framework, causality from variable x_i to variable x_j can be assessed if we can predict some information on $x_i(t)$ from $(x_j(t), x_j(t-1), \dots, x_j(t - E_{\text{optimal}} + 1))$. The cause variable x_i is generally referred to as the target variable, and the consequence variable x_j is the library variable. For each focal time t^*, we can predict the target variable $x_j(t^*)$ at a given time $t^* \geq E_{\text{optimal}}$ based on the $E_{\text{optimal}} + 1$-nearest neighbours of $(x_j(t^*), x_j(t^* - 1), \dots, x_j(t^* - E_{\text{optimal}} + 1))$ among all other data points in the lag space $\left((x_j(t), x_j(t-1), \dots, x_j(t - E_{\text{optimal}} + 1))\right)_{t \neq t^*\,,\, E_{\text{optimal}} \leq t \leq T}$. This means using a library size $L = T - E_{\text{optimal}}$ ($T - E_{\text{optimal}}$ points considered in the lag space) to find the corresponding time steps $t^{(1)}, \dots, t^{(E_{\text{optimal}}+1)}$ of the nearest neighbours in order to predict $\hat{x}_i(t^*)$ as a weighted average of the $x_i(t^{(1)}), \dots, x_i(t^{(E_{\text{optimal}}+1)})$. Similar to the Simplex projection described above, we define a forecasting skill ρ as the correlation between the observed $\left(x_i(t^*)\right)_{E_{\text{optimal}} \leq t^* \leq T-1}$ and the predicted $\left(\hat{x}_i(t^*)\right)_{E_{\text{optimal}} \leq t^* \leq T-1}$ over all focal time steps t^*. We can repeat this set of predictions for various library sizes L by randomly picking L time steps that will be the only ones considered for the nearest neighbours. We applied 100 bootstraps of this random subsample of time steps for 20 library sizes L regularly distributed from 5 to $T - E_{\text{optimal}}$. Since the CCM relies on E_{optimal} for the library variable, if no embedding dimension was found relevant in the Simplex projection, no causality can be assessed from any variable to this library variable.

The causality was assessed in two successive tests detailed below. First, the assessment of causality requires an increase in the forecasting skill ρ with increasing library sizes L [27]. We applied a Mann–Kendall test [28] to check for a monotonic increase in the median of the forecasting skill over the 100 bootstraps along the library size, that is on $L \mapsto \text{median}\left\{\rho(\text{library set})\right\}_{\text{library size}=L}$. If $\tau > 0$ and p-value < 0.05, the first step of the procedure is considered successful [23].

To ensure that the forecasting skill $\rho(L)$ resulted from the temporal structure of the time series, we compared the output of the CCM from the original time series to the output of a null model [27,29]. We generated surrogate time series by randomly shuffling time for the cause and the consequence variables: given a permutation σ of $\{1, \dots, T\}$, we considered the time series $x_i(\sigma(1)), \dots, x_i(\sigma(T))$ and $x_j(\sigma(1)), \dots, x_j(\sigma(T))$. We applied CCM to compute a forecasting skill for each library size across all 100 surrogate time series, using a single bootstrap per surrogate. Then, the second test to assess causality was passed if the median forecasting skill in the original time series was higher than the 95th percentile forecasting skill in the surrogates, for at least 18 out of 20 library sizes.

If both the Mann–Kendall test and the comparison with surrogates were passed, we concluded that there is causality from x_i to x_j. An example of CCM that passed both tests, and another that failed both tests is presented in figure 2. The CCM was applied using the `CCM` function from the R package `rEDM`. In addition, to compare our causality assessment with earlier CCM applications, we replicated the SST-recruitment (R) analysis of [23] for the 17 stocks considered in that study, applying the same CCM procedure and our two-step significance testing. This robustness comparison is summarized in table S1 in the supplementary material.

Note that CCM should be able to distinguish causality between a variable a and another variable b, from causality of a third variable c forcing both variables a and b [18]. We assessed causality from SST to SProd and from HRate to SProd. For a consistency check, we also assessed causality from SProd to SST and from SProd to HRate—which are not expected to occur.

2.4. Quantification of the causal effect: multivariate S-map forecasting

We applied the multivariate S-map forecasting to quantify the strength of causality for pairs of variables, where we identified causality using CCM (see the section above) [16,30]. The multivariate S-map aims at linearly approximating the dynamics in an embedding relevant for the causality we consider. The embedding should be of dimension E_{optimal} of the library variable (consequence variable) since it is better suited for studying the corresponding causality. This embedding space to study the strength of causality from x_i to x_j contains values associated with each time step t, starting with the dimensions $x_i(t)$ the cause variable at time t, $x_j(t)$ the consequence variable at time t. Then, if $E_{\text{optimal}} > 2$, we also consider the third variable at time t if the causal relationship was found significant for the third variable causing x_j. If the number of variables does not reach E_{optimal}, we add the lags of the consequence variable $x_j(t-k)$ for $k \in \mathbb{N}^*$ from 1 until the number of variables in the embedding reaches E_{optimal} [15,31].

Let us note $z_1, \dots, z_{E_{\text{optimal}}}$ the scaled variables in this embedding ($z_1 = \frac{x_i - \text{mean}_t(x_i)}{\text{std}_t(x_i)}$, $z_2 = \frac{x_j - \text{mean}_t(x_j)}{\text{std}_t(x_j)}$, and the other variables as explained above). For each focal time t^*, the dynamics $z_2(t^*+1) = g\left(z_1(t^*), \dots, z_{E_{\text{optimal}}}(t^*)\right)$ is linearly approximated by $z_2(t^*+1) \approx c_0^{(t^*)} + c_1^{(t^*)}\, z_1(t^*) + \cdots + c_{E_{\text{optimal}}}^{(t^*)}\, z_{E_{\text{optimal}}}(t^*)$. The coefficients $c_0^{(t^*)}, \dots, c_{E_{\text{optimal}}}^{(t^*)}$ are fitted using all time steps in a weighted linear regression, with weights decreasing exponentially:

$$w_t^{(t^*)}\, Z_2(t+1) = w_t^{(t^*)} c_0^{(t^*)} + w_t^{(t^*)} c_1^{(t^*)}\, Z_1(t) + w_t^{(t^*)} c_2^{(t^*)}\, Z_2(t) \;+\; \dots \;+\; w_t^{(t^*)} c_{E_{\text{optimal}}}^{(t^*)}\, Z_{E_{\text{optimal}}}(t) + \epsilon_{t^*}, \tag{2.1}$$

$$\text{with} \quad w_t^{(t^*)} = \exp\left\{ -\theta \frac{||\mathbf{z}(t) - \mathbf{z}(t^*)||}{\frac{1}{T}\sum_{l=1}^{T} ||\mathbf{z}(l) - \mathbf{z}(t^*)||} \right\}, \quad \text{noting} \quad \mathbf{z} = (z_1, \dots, z_{E_{\text{optimal}}}), \tag{2.2}$$

where $t \in \{1, \dots, T\}$ are all the time steps, $c_0^{(t^*)}, \dots, c_{E_{\text{optimal}}}^{(t^*)}$ are the parameters of the regression for the focal time step t^*, $\left(w_t^{(t^*)}\right)_{t \in \{1,\dots,T\}}$ are weights at focal time t^* decreasing exponentially with a nonlinear parameter θ —representing how local is the information in

Downloaded from royalsocietypublishing.org/rsif/article-pdf/doi/10.1098/rsif.2025.1040/6157114/rsif.2025.1040.pdf
by guest
on 15 August 2026

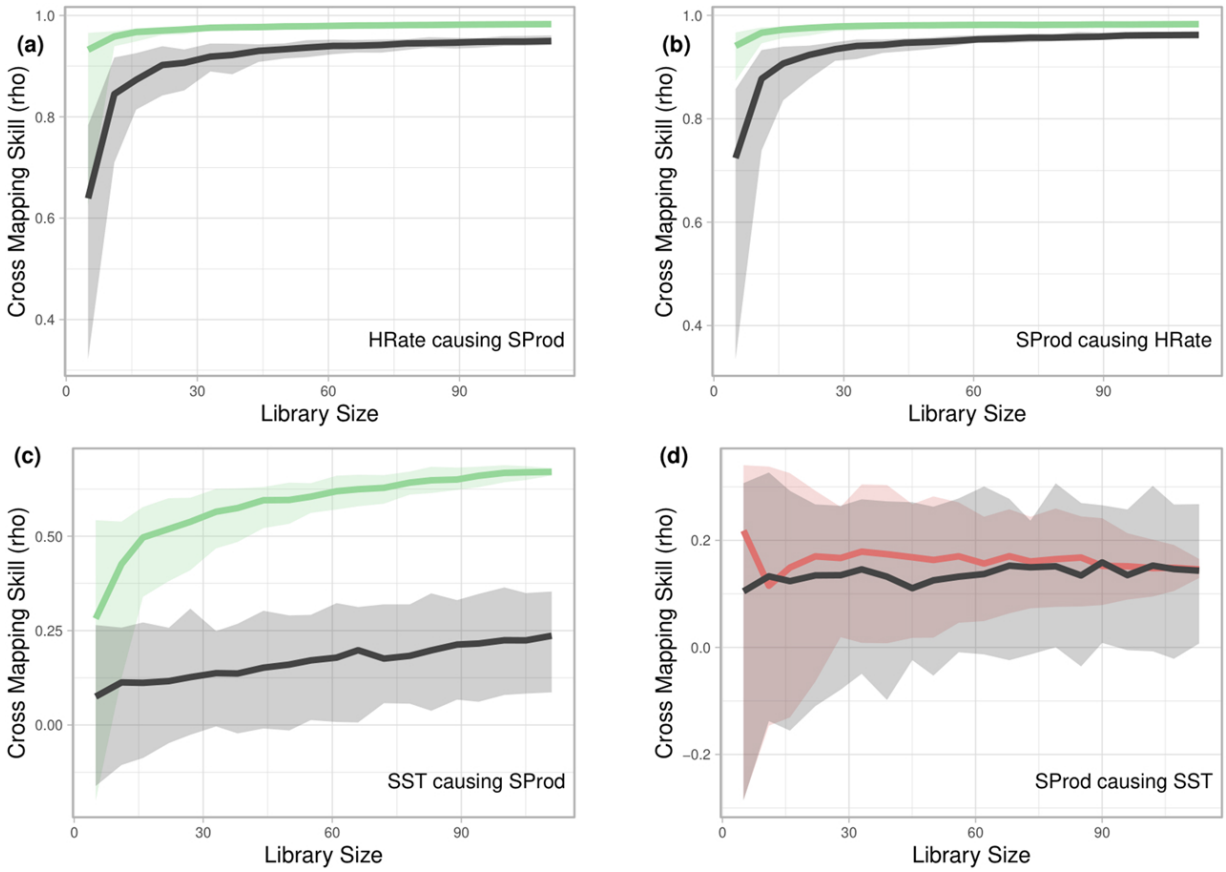


Figure 2. Convergence in the CCM for all causal relationships tested for the stock *China rockfish Southern Pacific Coast*. Both directions of causality are tested: HRate (target variable) causing SProd (library variable) (a), SProd (target variable) causing HRate (library variable) (b), SST (target variable) causing SProd (library variable) (c) and SProd (target variable) causing SST (library variable) (d). The green (respectively, red) curves correspond to the CCM on the original data with 100 bootstraps (solid line for the median and ribbon for the 5th and 95th percentiles of the bootstraps) when causality was identified (respectively, not identified). It represents the forecasting skill of the target variable given a number of points included in the library variable. The grey curves correspond to the 100 surrogates (solid line for the median and ribbon for the 5th and 95th percentiles of the surrogates). Mann–Kendall's τ are $\geq$ 0.999, 0.958, 0.999 and −0.400 with corresponding p-values of $\leq 10^{-6}$, $\leq 10^{-6}$, $\leq 10^{-6}$ and 0.015 for (a), (b), (c) and (d), respectively. Median forecasting skill is higher than the 95th percentile of the surrogates for all of the 20 library sizes for (a), (b) and (c) and for none of the library sizes for (d).

the manifold of the embedding space. We applied the S-map with θ between 0 and 20 in increments of 0.2 — $Z_1(t), \ldots, Z_{E_{\text{optimal}}}(t)$ are the random variables with realizations $z_1(t), \ldots, z_{E_{\text{optimal}}}(t)$ and $\epsilon_{t^*} \sim \mathcal{N}\left(0, \eta^{(t^*)}\right)$ the residual. It can be viewed as a weighted least-squares regression for each focal time t^*, with weights $\left(w_t^{(t^*)}\right)^2$ for each individual t. We then chose θ that provided the highest forecasting skill—defined as the correlation between the observed $\left(z_2(t^*+1)\right)_{t^*}$ for t^*, where all $z_j(t^*)$ are defined and the predicted $\left(\hat{z}_2^{(t^*)}(t^*+1)\right)_{t^*}$ for t^*, where all $z_j(t^*)$ are defined. The multivariate S-map forecasting was applied using the `SMap` function from the R package `rEDM`.

The coefficient $c_1^{(t^*)}$ is therefore the S-map coefficient, informing on the strength of causality from x_i to x_j at time t^*. We applied a t-test on the coefficients $\left(c_1^{(t^*)}\right)_{t^* \in \{1,\ldots,T-1\}}$ to identify a non-significant sign (p-value > 0.05), a positive sign (p-value $\leq$ 0.05 and positive mean) and negative sign (p-value $\leq$ 0.05 and negative mean) of the S-map coefficients. We also applied a linear regression on $\left(c_1^{(t)}\right)_{t \in \{1,\ldots,T-1\}}$, depending on t, to identify a non-significant trend (p-value > 0.05 of the model), a positive trend (p-value $\leq$ 0.05 and positive linear coefficient on t) or a negative trend (p-value $\leq$ 0.05 and negative linear coefficient on t) of the S-map coefficient. An example of the coefficients along time, t-test and linear regression is presented in figure 3. Note that even when causality is detected, the S-map coefficient may not exhibit a statistically significant sign (based on a t-test) or a significant linear trend over time. This can occur because the strength may be stable, change nonlinearly or change sign.

3. Results

3.1. Causality assessments in fish stock trajectories

The CCM analysis was applied to a dataset of 155 fish stocks to identify causal relationships between stock productivity and its potential drivers: fishing pressure (HRate harvest rate) and SST. The results, summarized in figure 4a, indicate that fishing pressure (harvest rate) was the most frequently detected causal driver of productivity. A significant causal link from harvest rate to productivity (HRate to SProd) was identified in 71 of the 155 stocks analysed (45.8%). By contrast, a causal influence of SST on

Downloaded from royalsocietypublishing.org/rsif/article-pdf/doi/10.1098/rsif.2025.1040/6157114/rsif.2025.1040.pdf
by guest
on 15 August 2026

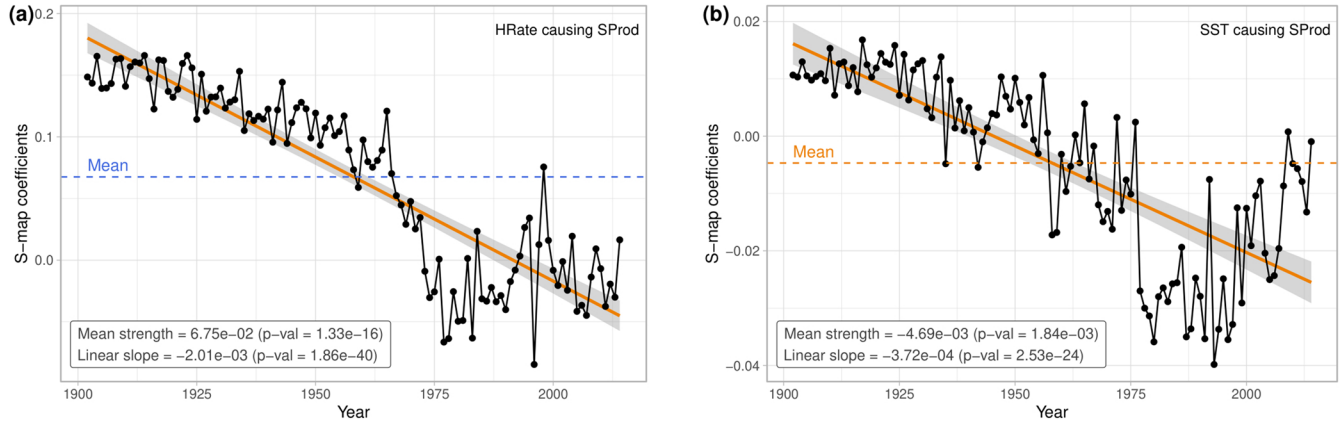


Figure 3. S-map coefficients along time for the causality from HRate to SProd and from SST to SProd for the stock *China rockfish Southern Pacific Coast*. Both *t*-tests and linear regressions are considered significant, providing a positive mean of 6.75×10^{-2} and a decreasing trend of -2.01×10^{-3} year^{-1} for the causality from HRate to SProd, and a negative mean of -4.69×10^{-3} and a decreasing trend of -3.72×10^{-4} year^{-1} for the causality from SST to SProd. The values are without the unit of the variables since they are scaled for the S-map forecasting. This could be interpreted as an average positive effect of HRate on SProd decreasing over time and turning negative, and an average negative effect of SST on SProd starting positive and becoming more negative over time.

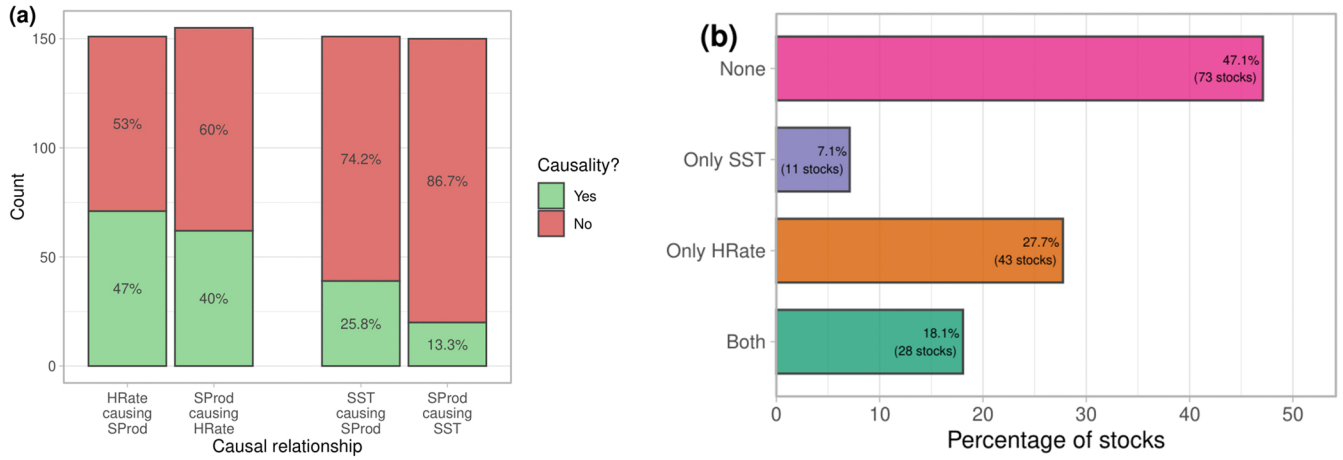


Figure 4. CCM results for the detection of causal relationships. (a) Stacked bar plot of the number of stocks, where the causality is assessed for each causal relationship tested. Stocks for which causality was deemed irrelevant were removed from the bars, corresponding to four stocks for SST causing SProd and HRate causing SProd and five stocks for SProd causing SST. In these cases, the library variable (consequence variable, here SProd and SST) did not provide a reliable embedding, as indicated by negative forecasting skill in the Simplex projection. (b) Horizontal bar plot of the percentage (and number) of stocks in the joint causality category for SST → SProd and HRate → SProd (both, only SST, only HRate, none).

productivity (SST to SProd) was found in 39 stocks (25.2%). The analysis also tested for reverse causality, finding that productivity was a driver of the harvest rate in 62 stocks (40%) and of SST in only 20 stocks (13.3%), suggesting that drivers primarily influence productivity rather than the other way around (as expected). Figure 4b shows the distribution of causality detection results across 155 fish stocks, categorized by the drivers that showed significant causal relationships with stock productivity. Among stocks with detectable causality, harvest rate emerged as a more prevalent driver than SST: 43 of stocks showed causality only with harvest rate, while 11 exhibited causality only with SST. A smaller proportion of stocks (28) demonstrated significant causal relationships with both environmental drivers.

As a robustness comparison to prior CCM work, we also re-analysed the 17 SST-recruitment pairs previously examined [23] using our stricter two-step CCM significance criteria. Under this framework, we detected a significant SST to R causal link only for Eastern Atlantic bluefin tuna, whereas the remaining stock-SST combinations did not pass our thresholds (table S1 in the supplementary material). This confirms that our implementation is conservative relative to earlier applications while reproducing the strongest previously reported signal.

3.2. Estimations of causal signs and trends

Following the detection of causal links of SST and HRate on SProd, a multivariate S-map analysis was conducted to quantify the strength, sign and temporal trend of these relationships (figure 5). Of the stocks analysed, a majority (23 stocks) showed a significantly negative average effect of SST on SProd (figure 5). By contrast, eight stocks exhibited a positive effect and eight

Downloaded from royalsocietypublishing.org/rsif/article-pdf/doi/10.1098/rsif.2025.1040/6157114/rsif.2025.1040.pdf
by guest
on 15 August 2026

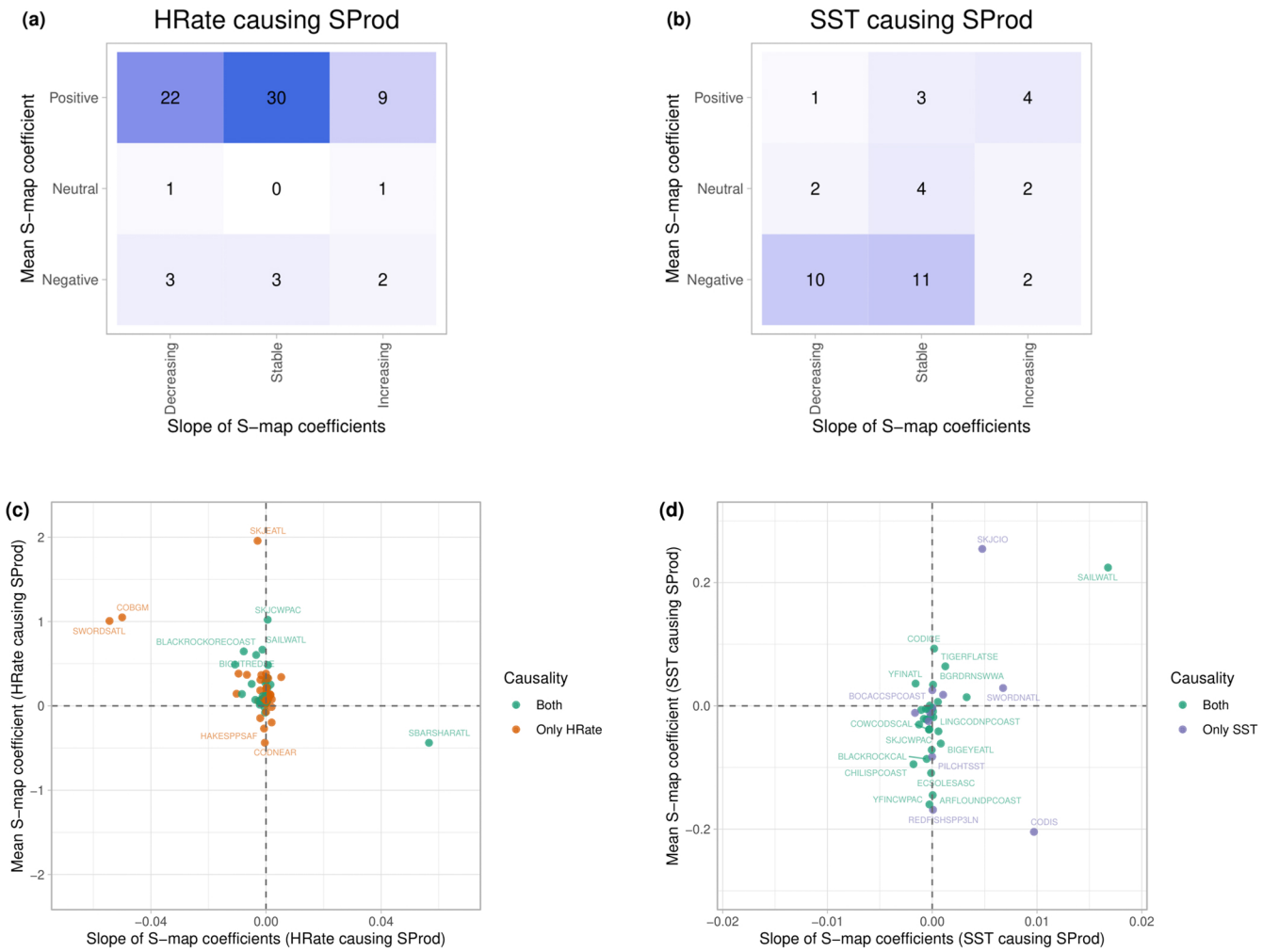


Figure 5. Sign and trend of the causal effects, resulting from the analysis on the multivariate S-map. These results are only provided for stocks where causality was assessed (figure 4). (a) and (b) Sign and trend of the S-map coefficients, for the causal relationship from HRate to SProd (a) and from SST to SProd (b). (c) and (d) Scatter plots of the sign versus trend of the S-map coefficients for each stock, for HRate causing SProd (c) and SST causing SProd (d). Labels in the graph are stock IDs.

showed no significant average sign. The strength of the causal link from SST to SProd did not change significantly over time for 18 stocks. However, a notable number of stocks displayed a significant trend; the effect became increasingly negative over time for 13 stocks and more positive for eight stocks. The most common patterns observed in 11 stocks were a significantly negative causal effect that remained stable over time, followed by 10 stocks with a negative effect that grew significantly stronger (more negative) over the time series.

For the causal link from harvest rate to productivity, the S-map analysis indicated a mostly positive response among the stocks (figure 5). A significantly positive effect of harvest rate on productivity was identified in 61 stocks, suggesting that for these populations, increasing fishing pressure was associated with higher productivity. Conversely, eight stocks showed a significantly negative relationship, where higher harvest rates corresponded to lower stock productivity. For the remaining two stocks, the S-map coefficient for the effect of harvest rate was not statistically significant. The scatterplots of S-map coefficient mean strength and temporal slope (figure 5c,d) reveal that harvest rate effects on productivity for most are tightly clustered around zero with relatively modest temporal variation, whereas SST effects exhibit a tighter coefficient range. Together, these patterns indicate that both the mean effect and its temporal change are stronger for harvest rate than for SST in shaping stock productivity.

To explore the stock-status dependence of the HRate to SProd causal effect, we plotted the mean S-map coefficient against the log-transformed average B/B_{MSY} for each stock (figure S5 in the supplementary material). Stocks with lower relative biomass tended to show weaker or negative HRate effects on productivity, while stocks at or above $B/B_{MSY} = 1$ showed predominantly positive effects, consistent with the ascending limb of the surplus production curve, where moderate exploitation stimulates productivity. A generalized linear mixed model (GLMM) confirmed a significant positive relationship between $\log B/B_{MSY}$ and the mean S-map coefficient (slope = 0.25), though the low marginal $R^2 = 0.03$ relative to the conditional $R^2 = 0.61$ indicates that while stock status is a detectable predictor, stock-specific characteristics account for the majority of variability in causal effect strength. Individual stock-level results are provided for readers to inspect specific cases (figures S6–S8 in the supplementary material). Additionally, the slopes of the relationship between S-map coefficients and $\log B/B_{MSY}$ were predominantly positive across stocks, and those positive slopes were associated with larger R^2 values (figure S9 in the supplementary material).

Downloaded from royalsocietypublishing.org/rsif/article-pdf/doi/10.1098/rsif.2025.1040/6157114/rsif.2025.1040.pdf
by guest
on 15 August 2026

Spatially, the maps in figure S10 in the supplementary material revealed pronounced spatial heterogeneity in both the sign and temporal trend of the effects: for SST → SProd, many regions are dominated by negative coefficients that are either stable or becoming more negative, with positive or neutral slices occurring more sporadically across the global distribution. In regions with multiple assessed stocks, such as the US West Coast, the Atlantic Ocean and Australia, the SST signal tends to cluster in negative-stable or negative-decreasing categories, whereas regions represented by one or two stocks show mixed signs and trends that warrant cautious interpretation. By contrast, the HRate → SProd maps exhibit predominantly positive effects in many regions—often with stable or increasingly positive trends—while negative responses are present in a minority of areas and typically display stable or decreasing trends. Collectively, these spatial patterns underscore region-dependent dynamics in both sign and trend, with clearer regional signals emerging where local sample sizes are larger and more heterogeneous mosaics where representation is sparse.

To explore whether life history traits mediate the sensitivity of stocks to climate and exploitation, we tested for differences in functional traits across causality assessment outcomes, sign and temporal trend of S-map coefficients (figures S12–S14 and table S3 in the supplementary material). Among the four significant pairwise differences detected, higher trophic level species were more frequently associated with causal relationships from both SST and HRate to SProd. Additionally, stocks with a significantly negative trend in the SST to SProd S-map coefficient tended to have longer lifespans, as indicated by greater maximum age and lower natural mortality, suggesting that long-lived species may be particularly vulnerable to the intensifying negative effects of ocean warming on productivity.

4. Discussion

This study applied a data-driven framework to assess the causal effect of fishing pressure and warming on fish stock productivity on a global scale. Using EDM, our analysis showed that the causal effect of both drivers varies by stock, but identified harvest rate as the most prevalent driver of stock productivity, a finding that aligns with global syntheses that identify direct exploitation as the leading driver of productivity and biodiversity loss in marine ecosystems, ahead of climatic and other types of pressures [4,32]. The influence of SST was detected in a substantial number of stocks (25.2%), providing data-driven evidence that climate forcing directly impacts the productivity of fisheries. These results underscore the value of equation-free methods for disentangling the complex, nonlinear interactions that govern fisheries dynamics, moving beyond traditional models that may struggle to capture such complexity [22,33,34].

Our analysis of the quantified causal effects revealed distinct patterns for management. The influence of harvest rate on productivity was divided: for some stocks, higher fishing pressure was linked to increased productivity, while for others it was associated with a decline. This dual effect is consistent with fisheries theory, where productivity may initially rise with exploitation before declining as a stock becomes overfished [10,11]. However, a mean positive Smap coefficient does not necessarily mean that keeping fishing pressure will continue having a positive effect. As shown for the China Rockfish Southern Pacific Coast stock in figure 3, the sign of the Smap coefficient is significantly positive on average, but it crashes in the 1970s, reaching negative values. This highlights the relevance of assessing both the overall causal strength and its trend over time. More critically, the effect of SST on productivity was predominantly negative and, for many stocks, was found to be intensifying over time. This trend suggests that the adverse impacts of ocean warming on fish stocks are not only present but are becoming stronger, posing a growing threat to fisheries sustainability and food security [7,35,36]. This dynamic, non-stationary nature of environmental impacts highlights the limitations of static management approaches and points to the need for adaptive strategies that can account for changing environmental baselines [37].

Our findings on SST causality reveal several patterns when examined alongside previous research. Pierre *et al.* [23] analysed the causal link between SST and Recruitment (R) for 17 stocks, identifying significant relationships in 10 cases. When applying our more stringent approach to the same SST → R causal link, we detected causality only for Eastern Atlantic bluefin tuna (*Thunnus thynnus*). This result reflects the conservative nature of our methodology. Our primary analysis examined the link between SST and SProd across multiple fish stocks. We detected causal relationships for Baltic cod (*Gadus morhua*) and Irish Sea cod, consistent with findings by Pierre *et al.* for these species. For Iceland cod, we identified an SST →SProd link that had not been previously reported. However, several stocks showed no detectable SST → SProd relationship in our analysis, including Barents Sea cod, North Sea plaice (*Pleuronectes platessa*), and Arctic pollock (*Pollachius virens*). For Eastern Atlantic bluefin tuna, direct evaluation of SST → SProd links was not possible due to data limitations in our final dataset (table S1 in the supplementary material). The methodological approach employed in this study differs from previous work in its validation framework. Both studies utilize CCM, but our method incorporates an additional validation step: comparing observed forecast skill against null models generated from time-shuffled surrogates. This dual-test approach provides more stringent causality assessment, which accounts for the reduced number of significant causal links detected compared to methods that rely solely on convergence trend analysis. The uncovered mixture of positive and negative SST to SProd effects is consistent with thermal performance curve theory, where fish productivity peaks at a species-specific thermal optimum and declines at both lower and upper temperature extremes [38]. The dominance of negative and intensifying effects over time suggests that a growing proportion of stocks may already be operating above their thermal optima as oceans warm. Linking the sign and trend of SST effects to species-specific thermal thresholds would be a valuable avenue for future research to identify stocks most at risk. The association between higher trophic levels and a greater prevalence of causal links from both SST and HRate to SProd suggests that species occupying higher positions in the food web may integrate the effects of both climate and exploitation more strongly, possibly reflecting their dependence on prey dynamics that are themselves sensitive to these drivers. Moreover, the tendency for long-lived species to show increasingly negative SST effects over time further points to a life-history dimension of climate vulnerability that requires further investigation. Future work

Downloaded from royalsocietypublishing.org/rsif/article-pdf/doi/10.1098/rsif.2025.1040/6157114/rsif.2025.1040.pdf
by guest
on 15 August 2026

explicitly linking thermal performance curves, demographic buffering capacity and age-structured productivity to the sign and trend of driver effects would help clarify which life history strategies confer resilience or sensitivity to ongoing warming and fishing pressure.

While our approach offers a robust, equation-free method for assessing fishery dynamics, it is not without limitations. EDM methods are sensitive to time series length and the magnitude of observation error; they perform best with long time series and may struggle to resolve complex dynamics in short datasets or for species with lifespans longer than the available data (figure S11 in the supplementary material) [18,39]. Our analysis was also restricted to testing harvest rate and SST as drivers, while other factors such as predator–prey interactions, habitat quality or other environmental variables could also play crucial roles [4,15,31,34,40,41]. Moreover, stocks where causality was detected in both directions warrant particular caution, as Sugihara *et al*. note that shared external drivers—such as large-scale climate oscillations—can embed their signature into multiple time series simultaneously, producing apparent bidirectional CCM skill without implying true feedback between the variables [18]. A further limitation of our approach is that it does not explicitly account for age structure, which is a key determinant of stock productivity. Size-selective fishing progressively removes older, larger individuals, truncating the age distribution, and this can increase the sensitivity of productivity to both fishing pressure and environmental forcing. Future work incorporating age-structured productivity metrics would help disentangle the direct effects of harvest rate from those mediated by changes in population age structure.

Despite these limitations, our results illustrate how nonlinear, data-driven analyses can provide diagnostic indicators of how fishing pressure and temperature are associated with changes in stock productivity. By quantifying the strength and temporal evolution of these driver–productivity relationships, EDM-based indicators could be used alongside conventional assessments to flag potential shifts in productivity regimes and to generate hypotheses about the timing and direction of driver effects, rather than to directly evaluate the efficacy of specific management measures. Formal management strategy evaluation, which would require testing alternative harvest control rules and feedback in a simulation framework, is beyond the scope of this study.

Our empirical demonstration focuses on assessed stocks from the RAM Legacy database, and thus on systems that are already amenable to traditional stock-assessment models. The methodological framework, however, could in principle be extended to other data-rich cases where reasonably long time series of catches, biomass and environmental conditions exist, including situations where fitting process-based assessment models is difficult. Future research could explore such applications and test a wider array of biotic and abiotic drivers adapted to specific ecosystems, moving incrementally towards an ecosystem-based approach to fisheries management that is adaptive to a changing climate [42–45].

Ethics. This work did not require ethical approval from a human subject or animal welfare committee.

Data accessibility. Data and code to generate results and figures are available in Zenodo at [46].

Declaration of AI use. We have not used AI-assisted technologies in creating this article.

Authors' contributions. R.B.: conceptualization, data curation, formal analysis, investigation, methodology, software, visualization, writing—original draft, writing—review and editing; V.D.: conceptualization, funding acquisition, supervision, validation, writing—review and editing; A.VC.: conceptualization, investigation, methodology, supervision, validation, visualization, writing—original draft, writing—review and editing.

All authors gave final approval for publication and agreed to be held accountable for the work performed therein.

Conflict of interest declaration. We declare we have no competing interests.

Funding. This work was supported by the Agence Nationale de la Recherche (grant no. JCJC ANR-22-CE32-0001-01).

References

1. Food and Agriculture Organization of the United Nations. 2024 *The state of world fisheries and aquaculture 2024: blue transformation in action*. Rome: FAO.
2. Cooley S *et al*. 2023 *Oceans and coastal ecosystems and their services*. Cambridge, UK: Cambridge University Press.
3. Free CM, Thorson JT, Pinsky ML, Oken KL, Wiedenmann J, Jensen OP. 2019 Impacts of historical warming on marine fisheries production. *Science* **363**, 979–983. (doi:10.1126/science.aau1758)
4. Pélissié M, Devictor V, Jensen O, Dakos V. 2025 Ocean warming drives abrupt declines in fish productivity at global scale. *EcoEvoRxiv*. (doi:10.32942/x22s86)
5. Sailley SF *et al*. 2025 Multiple models of European marine fish stocks: regional winners and losers in a future climate. *Glob. Chang Biol.* **31**, e70149. (doi:10.1111/gcb.70149)
6. Teshome M. 2024 Charting the systemic and cascading impacts of climate change on marine food systems and human health. *BMJ Glob. Health* **8**, e014638. (doi:10.1136/bmjgh-2023-014638)
7. Boyce DG *et al*. 2022 A climate risk index for marine life. *Nat. Clim. Chang.* **12**, 854–862. (doi:10.1038/s41558-022-01437-y)
8. Hilborn R. 2001 Calculation of biomass trend, exploitation rate, and surplus production from survey and catch data. *Can. J. Fish. Aquat. Sci.* **58**, 579–584. (doi:10.1139/f01-018)
9. Vert-pre KA, Amoroso RO, Jensen OP, Hilborn R. 2013 Frequency and intensity of productivity regime shifts in marine fish stocks. *Proc. Natl Acad. Sci.* **110**, 1779–1784. (doi:10.1073/pnas.1214879110)
10. Barrowman NJ, Myers R. 1996 Is fish recruitment related to spawner abundance? *Fish. Bull.* **94**, 707–724.
11. Hilborn R *et al*. 2020 Effective fisheries management instrumental in improving fish stock status. *Proc. Natl Acad. Sci.* **117**, 2218–2224. (doi:10.1073/pnas.1909726116)
12. Bellard C, Marino C, Courchamp F. 2022 Ranking threats to biodiversity and why it doesn't matter. *Nat. Commun.* **13**, 1–4. (doi:10.1038/s41467-022-30339-y)
13. Brondízio ES, Settele J, Diaz S, Ngo HT. 2019 *Global assessment report of the Intergovernmental Science-Policy Platform on Biodiversity and Ecosystem Services*. Bonn: IPBES.
14. Griffith GP. 2020 Closing the gap between causality, prediction, emergence, and applied marine management. *ICES J. Mar. Sci.* **77**, 1456–1462. (doi:10.1093/icesjms/fsaa087)
15. Rigal S *et al*. 2023 Farmland practices are driving bird population decline across Europe. *Proc. Natl Acad. Sci.* **120**, e2216573120. (doi:10.1073/pnas.2216573120)
16. Sugihara G. 1994 Nonlinear forecasting for the classification of natural time series. *Phil. Trans. R. Soc. Lond. A* **348**, 477–495. (doi:10.1098/rsta.1994.0106)
17. Sugihara G, Grenfell BT, May RM, Tong H. 1997 Nonlinear forecasting for the classification of natural time series. *Phil. Trans. R. Soc. Lond. A* **348**, 477–495. (doi:10.1098/rsta.1994.0106)

Downloaded from royalsocietypublishing.org/rsif/article-pdf/doi/10.1098/rsif.2025.1040/6157114/rsif.2025.1040.pdf
by guest
on 15 August 2026

18. Sugihara G, May R, Ye H, Hsieh Ch, Deyle E, Fogarty M, Munch S. 2012 Detecting causality in complex ecosystems. *Science* **338**, 496–500. (doi:10.1126/science.1227079)
19. Ricard D, Minto C, Jensen OP, Baum JK. 2012 Examining the knowledge base and status of commercially exploited marine species with the RAM Legacy Stock Assessment Database. *Fish Fish.* **13**, 380–398. (doi:10.1111/j.1467-2979.2011.00435.x)
20. Vert-Pre KA, Amoroso RO, Jensen OP, Hilborn R. 2013 Frequency and intensity of productivity regime shifts in marine fish stocks. *Proc. Natl Acad. Sci.* **110**, 1779–1784. (doi:10.1073/pnas.1214879110)
21. Rayner N, Parker DE, Horton E, Folland CK, Alexander LV, Rowell D, Kent EC, Kaplan A. 2003 Global analyses of sea surface temperature, sea ice, and night marine air temperature since the late nineteenth century. *J. Geophys. Res. Atmos.* **108**, 4407. (doi:10.1029/2002jd002670)
22. Glaser SM, Ye H, Maunder M, MacCall A, Fogarty M, Sugihara G. 2011 Detecting and forecasting complex nonlinear dynamics in spatially structured catch-per-unit-effort time series for North Pacific albacore (*Thunnus alalunga*). *Can. J. Fish. Aquat. Sci.* **68**, 400–412. (doi:10.1139/f10-160)
23. Pierre M, Rouyer T, Bonhommeau S, Fromentin JM. 2018 Assessing causal links in fish stock–recruitment relationships. *ICES J. Mar. Sci.* **75**, 903–911. (doi:10.1093/icesjms/fsx202)
24. Takens F. 2006 Detecting strange attractors in turbulence. In *Dynamical systems and turbulence, Warwick 1980: proceedings of a symposium held at the University of Warwick 1979/80* pp. 366–381. Cham: Springer.
25. Deyle ER, Fogarty M, Hsieh Ch, Kaufman L, MacCall AD, Munch SB, Perretti CT, Ye H, Sugihara G. 2013 Predicting climate effects on Pacific sardine. *Proc. Natl Acad. Sci.* **110**, 6430–6435. (doi:10.1073/pnas.1215506110)
26. Edwards AM, Rogers LA, Holt CA. 2024 Explaining empirical dynamic modelling using verbal, graphical and mathematical approaches. *Ecol. Evol.* **14**, e10903. (doi:10.1002/ece3.10903)
27. Chang C, Ushio M, Hsieh C. 2017 Empirical dynamic modeling for beginners. *Ecol. Res.* **32**, 785–796. (doi:10.1007/s11284-017-1469-9)
28. Mann HB. 1945 Nonparametric tests against trend. *Econometrica* **13**, 245–259. (doi:10.2307/1907187)
29. Koutsodendris A *et al*. 2023 Atmospheric CO_2 forcing on Mediterranean biomes during the past 500 kyrs. *Nat. Commun.* **14,** 1664. (doi:10.1038/s41467-023-37388-x)
30. Deyle ER, May RM, Munch SB, Sugihara G. 2016 Tracking and forecasting ecosystem interactions in real time. *Proc. R. Soc. B* **283**, 20152258. (doi:10.1098/rspb.2015.2258)
31. Ushio M, Hsieh Ch, Masuda R, Deyle ER, Ye H, Chang CW, Sugihara G, Kondoh M. 2018 Fluctuating interaction network and time-varying stability of a natural fish community. *Nature* **554**, 360–363. (doi:10.1038/nature25504)
32. Jaureguiberry P *et al*. 2022 The direct drivers of recent global anthropogenic biodiversity loss. *Sci. Adv.* **8**, eabm9982. (doi:10.1126/sciadv.abm9982)
33. Hsieh Ch, Reiss CS, Hunter JR, Beddington JR, May RM, Sugihara G. 2006 Fishing elevates variability in the abundance of exploited species. *Nature* **443**, 859–862. (doi:10.1038/nature05232)
34. Tao HH, Hsieh Ch, Hidalgo M, Dakos V. 2025 Tracking changes in stability of North Sea Atlantic cod over 40 years. *ICES J. Mar. Sci.* **82**, fsaf117. (doi:10.1093/icesjms/fsaf117)
35. Boyce DG *et al*. 2024 Operationalizing climate risk in a global warming hotspot. *npj Ocean Sustain.* **3**, 33. (doi:10.1038/s44183-024-00067-5)
36. Free CM, Thorson JT, Pinsky ML, Oken KL, Wiedenmann J, Jensen OP. 2019 Impacts of historical warming on marine fisheries production. *Science* **363**, 979–983. (doi:10.1126/science.aau1758)
37. Free CM, Mangin T, Molinos JG, Ojea E, Burden M, Costello C, Gaines SD. 2020 Realistic fisheries management reforms could mitigate the impacts of climate change in most countries. *PLoS ONE* **15**, e0224347. (doi:10.1371/journal.pone.0224347)
38. Pörtner HO, Farrell AP. 2008 Physiology and climate change. *Science* **322**, 690–692. (doi:10.1126/science.1163156)
39. Perretti CT, Munch SB, Sugihara G. 2013 Model-free forecasting outperforms the correct mechanistic model for simulated and experimental data. *Proc. Natl Acad. Sci.* **110**, 5253–5257. (doi:10.1073/pnas.1216076110)
40. Lennox RJ *et al*. 2025 The role of habitat in predator–prey dynamics with applications to restoration. *Restoration Ecology* **33**, e14354. (doi:10.1111/rec.14354)
41. Hunsicker ME *et al*. 2011 Functional responses and scaling in predator–prey interactions of marine fishes: contemporary issues and emerging concepts. *Ecol. Lett.* **14**, 1288–1299. (doi:10.1111/j.1461-0248.2011.01696.x)
42. Cano AV, Jensen OP, Dakos V. 2025 Identifying fish populations prone to abrupt shifts via dynamical footprint analysis. *Proc. Natl Acad. Sci.* **122**, e2505461122. (doi:10.1073/pnas.2505461122)
43. Scotti M, Opitz S, MacNeil L, Kreutle A, Pusch C, Froese R. 2022 Ecosystem-based fisheries management increases catch and carbon sequestration through recovery of exploited stocks: the western Baltic Sea case study. *Front. Mar. Sci.* **9**, 879998. (doi:10.3389/fmars.2022.879998)
44. Holsman K *et al*. 2020 Ecosystem-based fisheries management forestalls climate-driven collapse. *Nat. Commun.* **11**, 4579. (doi:10.1038/s41467-020-18300-3)
45. Möllmann C, Cormon X, Funk S, Otto SA, Schmidt JO, Schwermer H, Sguotti C, Voss R, Quaas M. 2021 Tipping point realized in cod fishery. *Sci. Rep.* **11**, 14259. (doi:10.1038/s41598-021-93843-z)
46. Benerradi R, Dakos V, Cano AV. 2026 RaphBnrd/RAMLDB_causality: Accepted manuscript: Sensitivity of fish stock trajectories to climate forcing and human exploitation at a global scale. Zenodo. (doi:10.5281/zenodo.20594196).

Downloaded from royalsocietypublishing.org/rsif/article-pdf/doi/10.1098/rsif.2025.1040/6157114/rsif.2025.1040.pdf
by guest
on 15 August 2026